

---

# SUSCEPTIBILITY TO IMAGE RESOLUTION IN FACE RECOGNITION AND TRAINING STRATEGIES TO ENHANCE ROBUSTNESS

---

A PREPRINT

PUBLISHED IN LEIBNITZ TRANSACTIONS ON EMBEDDED SYSTEMS 2022

DOI: [HTTPS://DOI.ORG/10.4230/LITES.8.1.1](https://doi.org/10.4230/LITES.8.1.1)

 **Martin Knoche**  **Stefan Hörman**  **Gerhard Rigoll**

Chair of Human-Machine Communication

Technical University

Munich, Germany

[Martin.Knoche@tum.de](mailto:Martin.Knoche@tum.de)

November 28, 2022

## ABSTRACT

Face recognition approaches often rely on equal image resolution for verification faces on two images. However, in practical applications, those image resolutions are usually not in the same range due to different image capture mechanisms or sources. In this work, we first analyze the impact of image resolutions on the face verification performance with a state-of-the-art face recognition model. For images, synthetically reduced to  $5 \times 5$  px resolution, the verification performance drops from 99.23% increasingly down to almost 55%. Especially, for cross-resolution image pairs (one high- and one low-resolution image), the verification accuracy decreases even further. We investigate this behavior more in-depth by looking at the feature distances for every 2-image test pair. To tackle this problem, we propose the following two methods: 1) Train a state-of-the-art face-recognition model straightforward with 50% low-resolution images directly within each batch. 2) Train a siamese-network structure and adding a cosine distance feature loss between high- and low-resolution features. Both methods show an improvement for cross-resolution scenarios and can increase the accuracy at very low resolution to approximately 70%. However, a disadvantage is that a specific model needs to be trained for every resolution-pair. Thus, we extend the aforementioned methods by training them with multiple image resolutions at once. The performances for particular testing image resolutions are slightly worse, but the advantage is that this model can be applied to arbitrary resolution images and achieves overall a better performance (97.72% compared to 96.86%). Due to the lack of a benchmark for arbitrary resolution images for the cross-resolution and equal-resolution task, we propose an evaluation protocol for five well-known datasets, focusing on high, mid, and low-resolution images.

1

## 1 Introduction

In recent years, face recognition has gained progressively more attraction. Due to the availability of powerful GPUs and novel datasets with up to 87k identities, e.g. Microsoft's Celeb Dataset (MS1M) [1], research shifted more and more to deep-learning-based approaches. Nowadays, methods are generally based on the same principle as the method of choice: Representing the face using a deep convolutional neural network (DCNN) embedding. DCNNs are trained to map a facial image, typically after a pose alignment step, into a feature space such that intra-class distances are

---

<sup>1</sup>This work was partially supported by the *Bayerische Staatsministerium für Wirtschaft, Energie und Technologie* within the framework of a funding program of Informations- und Kommunikationstechnik for the project "Grundrechtskonforme Gesichtserkennung im öffentlichen Raum" (e-freedom).

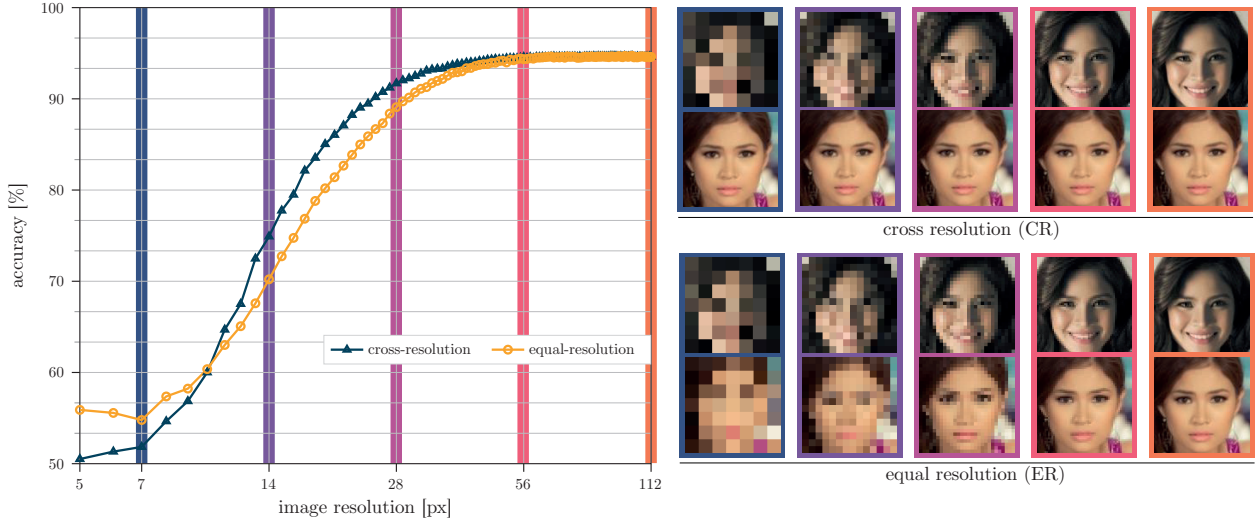


Figure 1: Average face verification accuracy across five popular datasets (LFW [13], AgeBDB [14], CFP-FP [15], CALFW [16] and CPLFW [17]) for cross-resolution and equal-resolution (left). Example image pairs are selected for five different resolutions (right).

minimized and inter-class distances are maximized. One of the first approaches was proposed by Szegedy *et al.* [2] in 2014 with a 9-layer convolutional neural network.

Typically, face recognition networks learn a projection into a distinct feature space according to their training dataset. Popular approaches are trained with datasets containing sufficient amount of high-resolution (HR) images. However, in real-world applications, the image quality is often inferior. Not only illumination conditions are different, also the resolution of a captured face can be of arbitrary size. For example, surveillance cameras capturing faces at very low resolutions, in contrast to very high-quality mug-shots-like passport images. Moreover, photos uploaded on social media platforms might show people in the background, hence, only tiny faces occur, which should also be recognized automatically by an algorithm. Current state-of-the-art approaches are susceptible against resolution and do not solve this problem satisfactorily. We analyze this in Sec. 4 more detailed. Many works [3, 4, 5] address low-resolution (LR) images for face recognition. However, they are using the same resolution for all test images. In real-world scenarios, image resolutions are likely different in the test setting. For example in social media networks people have a high resolution profile picture and should be recognized on photos, standing in the background, far away from the camera. Cross resolution (CR) face recognition is addressing the problem of comparing images with varying resolutions of images, which has yet found less attraction in the research. According to [6], existing approaches can be grouped into two methods: 1) Transformation-based approaches, on the one hand, aim to transform LR images to HR images via identity preserving super-resolution algorithms [7, 8, 9, 10]. In the opposite image resolution case, they perform simple down-sampling from HR to LR images. On the other hand, algorithms try to project extracted LR features into a HR feature space or vice-versa. 2) Non-transformation based approaches [11, 12] target to directly extract scale-invariant features into a common feature space.

In this work, we first investigate the behavior of a state-of-the-art face recognition network [18] on different resolution images for the verification task. We differentiate between a CR and LR verification scenarios in our analysis (*cf.* Fig. 1). Fig. 1 shows that the average performance (recognition accuracy) across several datasets strongly drops for CR and LR scenarios. At resolutions below  $10 \times 10$  px the accuracy is slightly above 50%, which is only barely about guessing. We are not concentrating at image resolutions lower than  $5 \times 5$  px. From this finding, we conclude that current state-of-the-art is susceptible against resolution and there is a huge gap for improvements, especially for very low image resolutions.

Other works addressing the CR problem are often dealing with exactly two resolutions in training and testing. However, this is not sufficiently transferable to real-world applications. Zeng *et al.* [12] use a mix of two and a mix of four resolutions, but they report only results in face identification scenarios. Therefore, we additionally experimented with multiple image resolutions for training. In general, we distinguish between two-resolution and multi-resolution training, which means on the one hand, precisely two different resolutions for training and on the other hand, numerous resolutions during training, respectively.

In summary, our main contributions are:

- We analyze the susceptibility for different image-resolution on face verification in-depth.
- We propose two intuitive, straightforward approaches and show performance improvements, especially for very low image resolutions.
- Moreover, we perform multi-resolution learning and show performance across several datasets.
- Lastly, we propose and publish three evaluation protocols focusing on low, mid and high resolution to measure the performance of multiple resolutions in the cross-resolution verification scenario. This is to our best knowledge the first benchmark for CR.

## 2 Related Work

### 2.1 Generic Face Recognition

Most face recognition methods in recent years focused on the networks loss to improve performance: FaceNet [19] proposed triplet loss in order to maximize the distances between the anchor image and it's positive sample. SphereFace [20] introduced angular softmax loss with a multiplicative angular margin, whereas CosFace [21] proposed an additive cosine margin. Finally, the authors of ArcFace [18] apply an Additive Angular Margin Loss function, which can effectively extent the discriminative power of features. Recently, Kim *et al.* [22] presented with GroupFace a novel architecture that utilizes multiple group-aware representations, to improve the quality of the feature. Wang *et al.* [23] proposed a hierarchical pyramid diverse attention network. The latter two methods clearly outperform the previously mentioned algorithms and become state-of-the-art.

### 2.2 Image Resolutions

To the best of our knowledge, there exists no dataset containing the same real-world face images in different resolutions for a comparatively large number of identities like the MS1M dataset. For analyzing the impact of resolutions, it is crucial to have the same photo in different resolutions. Naturally, a picture is taken in exactly one resolution. Hence there are no large datasets for this case available. This requires a synthetic downsample method, which can be applied onto arbitrary datasets. According to Zhou and Süssstrunk [24] a mapping from LR to HR images is often learned by synthetically downsampled HR images in order to retrieve training data for super-resolution approaches. They further state that the frequently used bicubic interpolation [25] significantly differs from real-world camera-blur.

### 2.3 Cross Resolution Face Recognition

As stated in Sec. 1, face recognition in the context of CR can be categorized into two groups: Transformation-based and non-transformation-based methods. Wang *et al.* [26] show an exhaustive review of those methods for addressing cross-resolution face-recognition. Fig. 2 gives a brief functional overview of those two methods.

#### Transformation-based Methods

These methods aim to focus on mapping images or extracted image features into a common feature space.

Lu *et al.* [27] presented a deep coupled ResNet model, containing one trunk network and two branch networks. The trunk network extracts features and the two branches networks transform HR and the corresponding LR features to a space where their difference is minimized.

Zangeneh *et al.* [28] proposed a two branch DCNN. While the LR branch consists of a super-resolution network combined with a feature-extraction network, the HR branch is only a feature-extraction network. Both branches are trained in three different training phases. For testing, images are fed through the branches depending on their resolution. A similar approach was used in [29], in which they trained a U-Net with a combination of reconstruction and identity preserving loss in order to super-resolve multi-scale low-resolution images. For feature extraction, they utilized a pretrained Inception-ResNet.

The authors of [30] proposed a coupled GAN-network structure, which comprises of two subnets, one for HR and one for LR. The correlation between from the subnet generated features is maximized. Moreover, they considered facial attributes, by implicitly matching facial attributes for both resolutions.

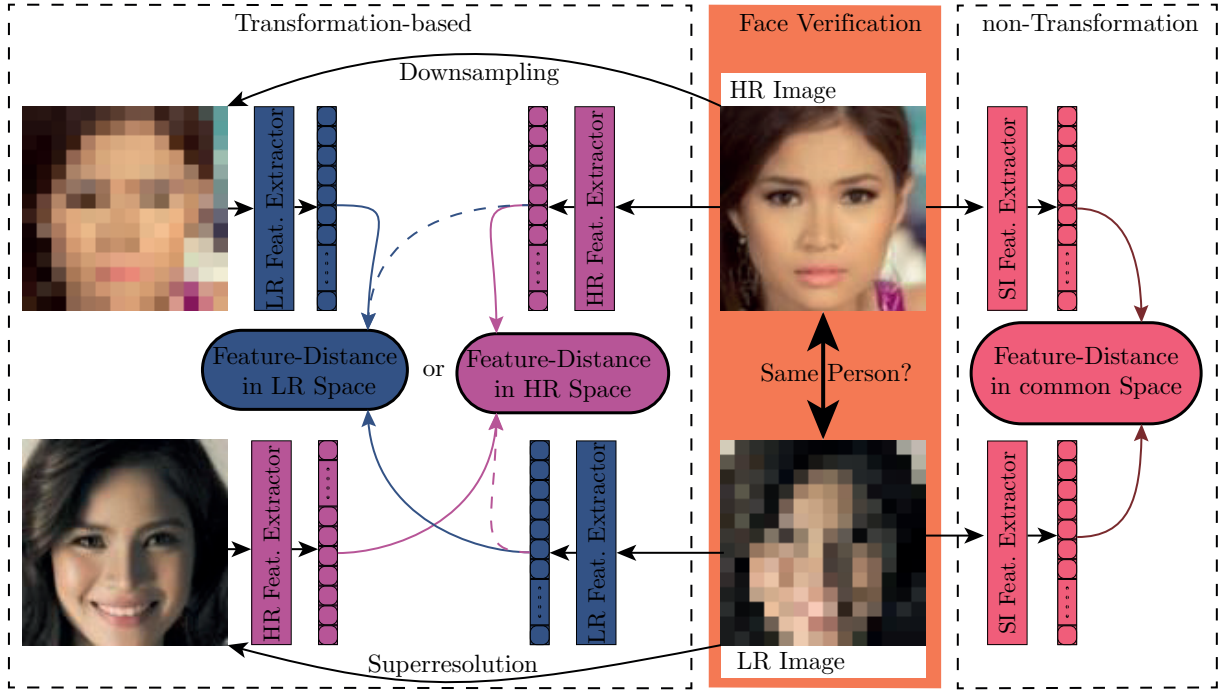


Figure 2: Methods in face recognition with CR images can be categorized into two folds: Non-transformation-based (right) approaches aim to learn directly scale-invariant image features. Transformation-based approaches (left) try to project learned image features or the images themselves to a common space.

### Non-Transformation-based Methods

Those techniques try to directly project features from arbitrary image resolutions into the same space.

In [12], Zeng *et al.* presented a resolution-invariant deep network and trained it directly with unified LR and HR images. However, they used only resolutions in the range of 24 to 60 pixels.

Massoli *et al.* [11] proposed a student-teacher network approach. They showed that their approach can be more effective concerning to preprocessing images with super-resolution techniques.

The authors of [31] showed that their DCNN architecture can address the problem of CR face recognition. They came up with a two-branch network architecture with several loss functions, which are trained on scale-invariant features for positive and negative sample pairs.

In [32], Ge *et al.* focused on low computational costs in low-resolution face recognition. Therefore they introduced a new learning approach via selective knowledge distillation. A two-stream technique (large teacher model and a light-weight student model) is employed to transfer selected knowledge from the teacher model to the student model.

## 3 Experimental Setup

In this section, we first describe the structure and training process of the baseline network, which we will utilize for our analysis. Then we take a closer look at the five popular datasets we use for testing. After that, we focus on the downsampling method. Finally, we elaborate on our performance measurement method for face verification accuracy.

### 3.1 Baseline Network

As our baseline network, we choose a network structure comprising a modified ResNet-50 [33] as proposed in ArcFace [18], pretrained on ImageNet [34], and an ArcFace layer for classification.

The backbone network (ResNet-50) consists of 4 blocks, which are repeated several times and containing in total 50 convolutional layers. The image dimension within the layers is decreasing, and the image depth is increasing from  $112 \times 112 \times 3$  px input to  $4 \times 4 \times 2048$  px at the end.

After flattening this  $4 \times 4 \times 2048$  px output from the backbone network, dropout is added. A bottleneck layer (512-dimensional fully connected layer), which represents the extracted features and is used for testing, is added following [35, 20, 21]. Finally, a fully connected layer with the dimension of the number of identities in our training set (87k) is added. We apply Additive Angular Margin Loss [18] together with a cross-entropy classification loss to the network.

For training, we select the Microsoft MS1M [1] dataset containing about 5.8M images from about 87k identities. We perform random brightness and saturation variations, left-right flipping, and random cropping of images as data augmentation. All training parameters are set according to [18] except for a smaller batch-size of 128 due to hardware limitations. The learning rate is set to 0.01 and is decreased by a factor of 10 after epoch 9 and epoch 13. In total, we train for 16 epochs with momentum SGD optimizer. The dropout rate and weight decay are set to 0.5 and  $5 \cdot 10^{-4}$ , respectively.

### 3.2 Testing Datasets

For our analysis, we select five popular datasets for testing face verification performance:

- The Labeled Faces in the Wild dataset (LFW) [13] discovers 13233 images from 5749 identities. The evaluation protocol contains 6000 positive (*i.e.*, same identity) image pairs and 6000 negative (*i.e.*, different identity) image pairs.
- AgeDB [14] includes 16488 images of 568 various people. It addresses a huge variety of age from 1 to 101 years. The evaluation protocol defines 3000 positive and 3000 negative image pairs.
- The CFP-FP [15] dataset protocol defines 3500 positive and 3500 negative image pairs and compares frontal with profile images.
- The cross age labeled faces in the wild dataset CALFW [16] is a variant of LFW with focus on the age gap in positive image samples. It contains 3000 positive and 3000 negative image pairs.
- The CPLFW [17] in contrast to CALFW addresses pose variations and selects 3000 positive and 3000 negative image pairs with high pose variations within each image pair.

We use the aligned and cropped to  $112 \times 112 \times 3$  px version of all above-mentioned testing datasets. In this paper, we exclusively deal with images having equal width and height. For simplicity, we denote the image resolution by naming only the first dimension, *i.e.*, a resolution of 112 px defines a  $112 \times 112 \times 3$  px image.

### 3.3 Reduction of Image Resolution

The baseline network requires HR input images  $\mathbf{I}_{HR}$  of the size 112 px. We simulate a resolution-reduction by performing the following two steps. 1) Downsample  $F_{down,r}(\cdot)$  images to an image dimension  $r$  in pixels. 2) Subsequently, upsample  $F_{up,r}(\cdot)$  those images back to the original image dimension and denote the resulting low-resolution images as  $\mathbf{I}_{LR}$ . The complete process can be formulated as follows:

$$\mathbf{I}_{LR} = F_{up,112}(F_{down,r}(\mathbf{I}_{HR})) \quad (1)$$

For both sampling processes, bicubic interpolation [25] is applied. To reduce unwanted artifacts, typically stemming from the downsampling process, standard antialiasing techniques are also involved. In Sec. 4.1, we further investigate these effects.

Fig. 3 illustrates the synthetic image resolution reduction. The left image  $\mathbf{I}_{HR}$  is a sample taken from the MS1M dataset with a resolution  $r = 112$ . In the center one can see the downsampled image  $F_{down,14}(\mathbf{I}_{HR})$  with image dimension  $r = 14$ . Finally, the upsampled image  $\mathbf{I}_{LR}$  is shown on the right and has qualitatively considered an image resolution of  $r = 14$  but technically the same image dimension as the  $\mathbf{I}_{HR}$  image. As one can see, all the high-frequency information is removed by this synthetically resolution-reduction. Simultaneously, the image dimension is equal to the original image, which is the required image size for our networks.

### 3.4 Accuracy in Face Verification

We report accuracy in all experiments, which denotes the face recognition rate in terms of face verification. To calculate the accuracy value for a given dataset, we first take the cosine-distances  $d$  between features of every image pair  $(\mathbf{I}_1, \mathbf{I}_2)$

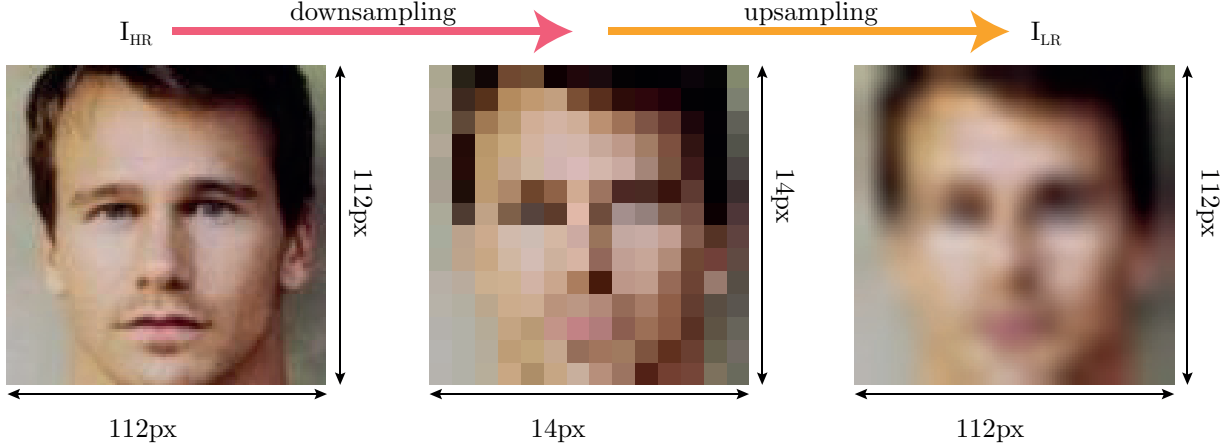


Figure 3: Illustration of the bicubic down- and up-sampling process to reduce the image resolution but keep the image dimension.

extracted from a model  $\mathcal{M}(\cdot)$  according to  $N$  image pairs defined in the specific evaluation protocol for each dataset respectively:

$$d = 1 - \sum \left( \frac{\mathcal{M}(\mathbf{I}_1)}{\|\mathcal{M}(\mathbf{I}_1)\|^2} \odot \frac{\mathcal{M}(\mathbf{I}_2)}{\|\mathcal{M}(\mathbf{I}_2)\|^2} \right) \quad (2)$$

Then, we use 10-fold cross-validation to find optimal thresholds that can separate feature distances of positive pairs (*i.e.*, same identity) from negative pairs (not same identity). The number of correctly identified positive samples and negative samples are then named as true positives  $TP$  and true negatives  $TN$ . We then calculate an accuracy score  $Acc$  as follows:

$$Acc = \frac{TP + TN}{N} \quad (3)$$

For all experiments in the CR scenario we generate two evaluation datasets by flipping the pairwise matching resolution from

$$(\mathcal{M}(\mathbf{F}_{up,112}(\mathbf{F}_{down,r}(\mathbf{I}_{HR,1}))), \mathcal{M}(\mathbf{I}_{HR,2}))$$

to

$$(\mathcal{M}(\mathbf{I}_{HR,1}), \mathcal{M}(\mathbf{F}_{up,112}(\mathbf{F}_{down,r}(\mathbf{I}_{HR,2}))))$$

We then calculate the accuracy score for both test datasets and then take the mean.

## 4 Analysis of Image Resolution Susceptibility

In this section, we first investigate the effect by reducing the resolution across five test datasets. Then, we investigate the performance of the baseline network under LR conditions in CR and ER scenarios. Afterward, we take a closer look at the extracted features, especially at the cosine distance between the image pairs, which is used to classify them as positive (same identity) or negative (different identity).

### 4.1 Effects of Resolution-Reduction on Datasets

To get a better insight of what is exactly happening when performing the synthetically reduction of image resolution, we elaborate on the difference between testing datasets. Hence, we calculate a mean image across the whole dataset and then highlight the mean pixel difference between LR and HR images. In Fig. 4 the left column shows a HR sample image  $\mathbf{I}_{HR}$  from MS1M and its corresponding reduced-resolution images  $\mathbf{F}_{up,112}(\mathbf{F}_{down,r}(\mathbf{I}_{HR}))$  for four resolutions

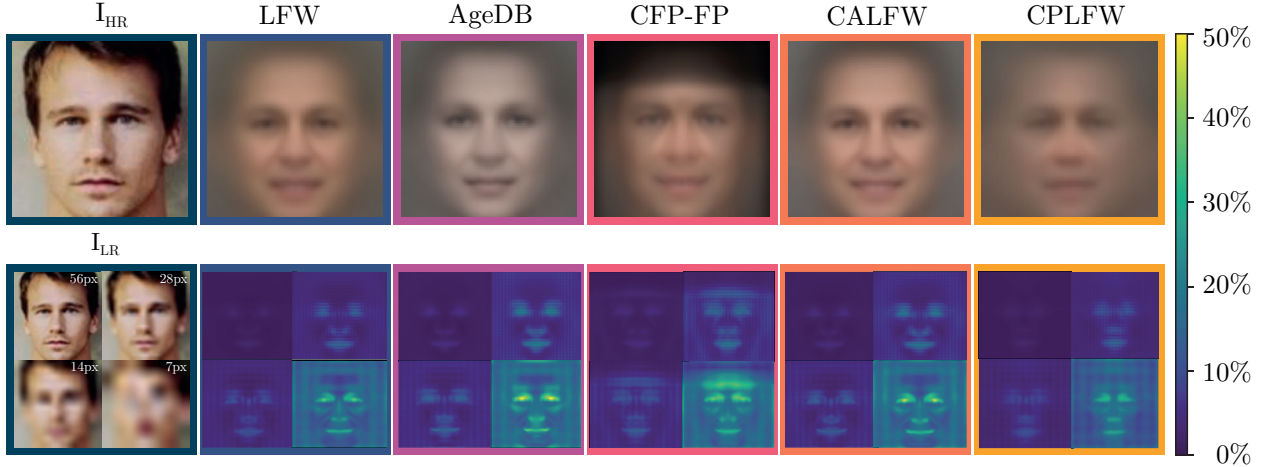


Figure 4: Illustration of the absolute pixel differences after the resolution-reduction process in comparison to the original HR images for several datasets. The left column illustrates the synthetically resolution-reduced images for one sample image picked from the MS1M datasets. The first row of all other images represents the mean image  $I_{HR}^{mean}$  for several datasets. Below are the pixel difference images  $D_r^{mean}$  for four specific resolutions  $r \in \{7, 14, 28, 56\}$ , for the same resolutions as in left-most column.

$r \in \{7, 14, 28, 56\}$ . All other columns show in the first row the mean HR image  $I_{HR}^{mean}$  for several datasets, which is derived as follows:

$$I_{HR}^{mean} = \frac{\sum_{i=1}^N I_{HR,i}}{N} \quad (4)$$

where  $N$  denotes the number of elements of the dataset.

Below each mean HR image, we denote the mean absolute pixel differences  $D_r$  between synthetically reduced images  $I_{LR,r}$ , and original  $I_{HR}$  images across each dataset. We retrieve those images for four resolutions  $r \in \{7, 14, 28, 56\}$  according to:

$$D_r^{mean} = \frac{\sum_{i=1}^N \left( \left| F_{up,112}(F_{down,r}(I_{HR,i})) - I_{HR,i} \right| \right)}{N} \quad (5)$$

As expected, eye, nose, and mouth regions are heavily affected by the resolution reduction process in all datasets. High detail information in those regions is lost. The maximum derivation of a single LR image pixel concerning its counterpart pixel in the HR image is about 50%. There are slightly visible artifacts in a grid style manner occurring in all pixel-difference images. These might still be some aliasing artifacts, which could not entirely be removed by the antialiasing method of the bicubic interpolation algorithm. The mean dataset HR images are quite different across all datasets. One can clearly see that pose variations in CPLFW dataset result in more blurred areas of the image. In contrast, the CALFW and LFW dataset images seem to be very accurately aligned and show almost a clear and detailed average face. Interestingly, the background in the CFP-FP dataset is very dark compared to other datasets. Also, the pose variation can be seen in the average face. Some ghosting effects are present in that image, too. In terms of pixel derivations, one can see that high-frequency information mainly in the region of eyes, nose, and mouth is lost during the resolution-reduction process. These are valuable information for face recognition. Thus, face verification performance is worse as we later see in the next section. All datasets show the same pattern with respect to their mean absolute pixel difference images. The variation is increasing for lower resolutions. This leads to the conclusion, that the image quality within each dataset is approximately equal.

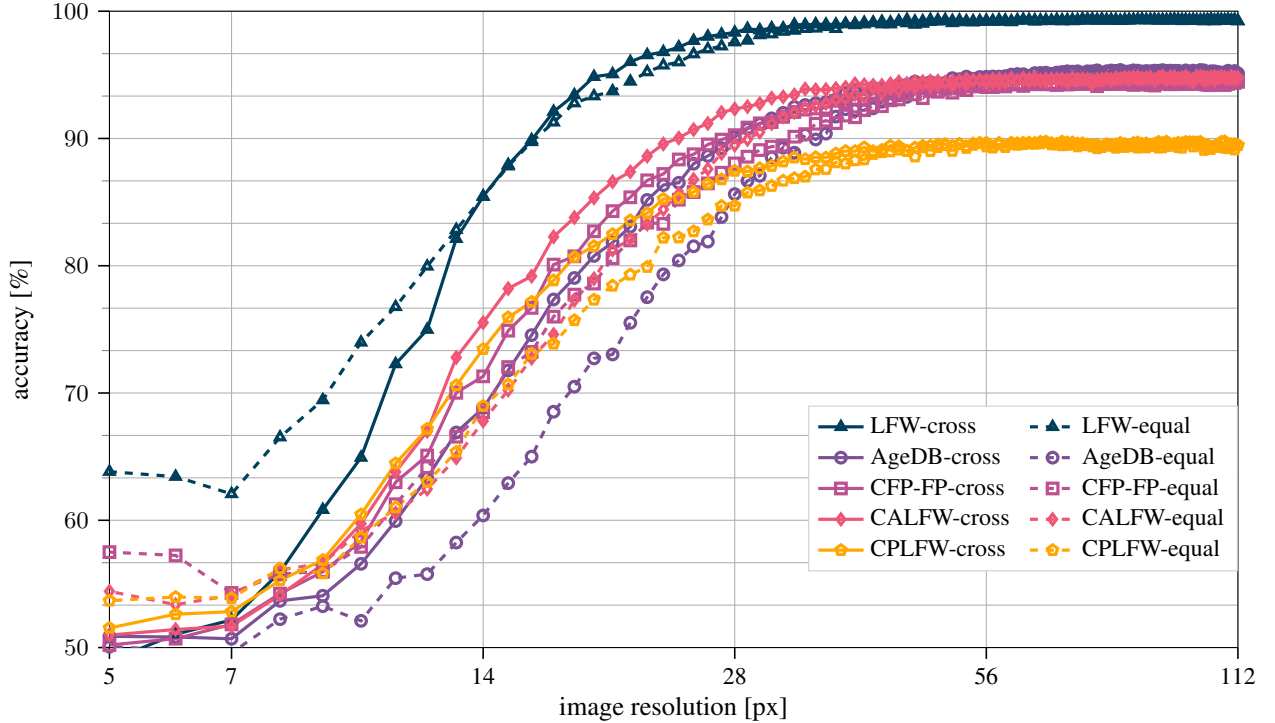


Figure 5: Face verification accuracy across several datasets for different image resolutions.

## 4.2 Face Verification Accuracy

Fig. 5 visualizes the accuracy for each of the in Sec. 3.2 introduced dataset across different image resolutions in CR (solid lines) and ER (dotted lines) scenario. The performance clearly drops as one would expect for lower resolutions. The best performance overall, but also the largest gap between CR and ER verification accuracy holds for the LFW dataset. In contrast to that, the baseline achieves worse performance on the CPLFW dataset, especially in the ER scenario. A reason for this can be the large pose variations, which are not occurring in the training dataset.

For a better understanding, what reasons are causing this large decrease of accuracy, we take a closer look at the extracted features from our baseline model in the next section.

## 4.3 Feature Distances

The distance between both feature vectors for a test image pair is, according to Equation (2), crucial for the verification accuracy. Hence, we plot in Fig. 6 the average feature distance for all positive image pairs and all negative image pairs in the LFW dataset for a given resolution. As stated in the previous section, we also consider this in the CR and ER scenario. One can divide the behavior roughly into three sections: 1) For high resolutions above about 60 px, feature distances between positive and negative image pairs seem to be independent of the image resolution. The average distance between positive pairs is quite low about 0.3 and the distance for negative pairs is about 1.0, which means that the high dimensional feature vectors are almost orthogonal. 2) Between resolutions of about 60 px and 20 px, which can be considered as mid-range resolutions, in both CR and ER scenarios, the distance of positive image pairs tends to increase. In contrast, the distance for negative image pairs stays at the same level. The most considerable mean feature distance for positive pairs in the ER scenario can be found at image resolutions about 19 px with a cosine distance of approximately 0.5. 3) The last section can be considered as low resolutions less than 20 px. Interestingly, distances for both scenarios show a contrary behavior. On the one hand, the mean feature distance for CR positive pairs is increasing towards 1. This is consistent with the accuracy decreasing towards about 50%, which is in terms of verification, merely guessing. On the other hand, in the ER case, positive and negative feature distances decreasing towards 0.1. This also coincides with low accuracy scores in that resolution range.



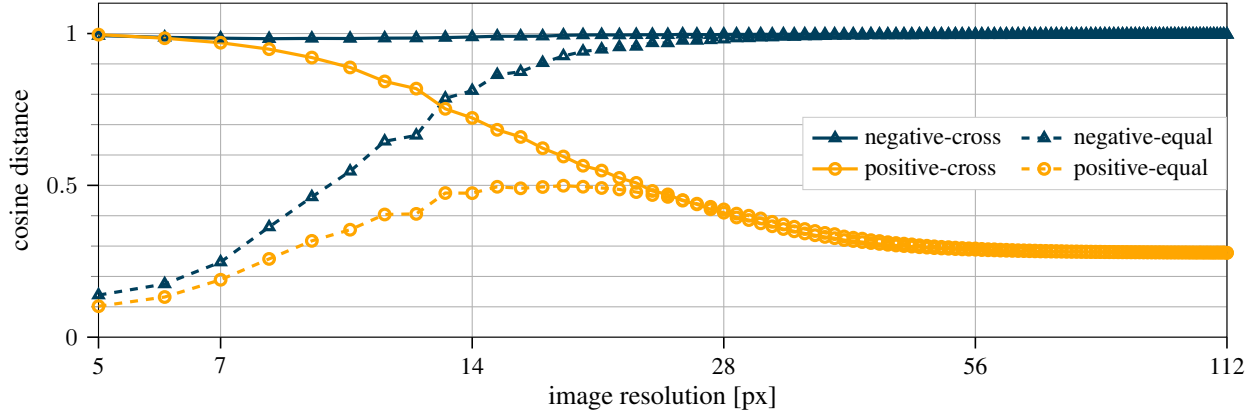


Figure 6: Average cosine feature distances between image pairs for positive (circles) and negative (triangles) pairs in the LFW dataset.

For the CR scenario, we conduct that our network is not able to extract accurate features for the very low resolution images. Hence, this results in a large distance between features because the HR image features are still very distinctive. However, in the ER scenario both images are somehow unfamiliar to the network and the extracted features are pretty similar. To underline this statement and analyze the distribution of features more fine-grained, we visualize the distributions of positive and negative feature distances for five specific image resolutions (7 px, 14 px, 28 px, 56 px, and 112 px). Fig. 7 is capturing those cosine feature distance distributions for the LFW dataset.

The center violin plots represent the feature distance distribution for HR image pairs. Distances for positive and negative image pairs are clearly distinguishable. The positive distances are mainly in a range between 0.1 and 0.6, whereas negative distances are mostly in the field of 0.6 and 1.4. Both classes can be separated effectively with a threshold of about 0.6, and thus, the accuracy for only HR images is best (cf. Fig. 5). To the left side, distributions for the CR scenario are shown. On the right side, ER feature distributions are plotted. In both procedures, for a image resolution of 56 px no significant difference can be noticed. Interestingly, the peak feature distance for positive image pairs even exceeds the maximum distance for negative pairs in the CR scenario at very low resolution 5 px. In other words, the resolution has a more enormous impact on the distance than the identity itself. The gap between CR and ER accuracy for very low resolutions is therefore reasonable. Despite of the small distances for both kinds of image pairs in the ER case, still more positive feature distances have a smaller value. This behavior explains a higher accuracy for very low

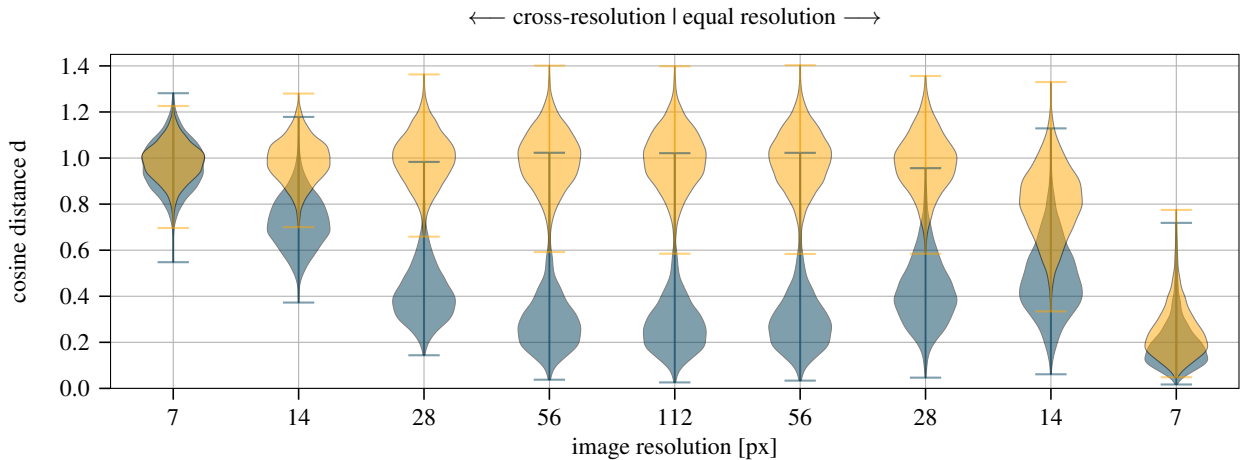


Figure 7: Cosine feature distance distributions for positive (blue) and negative (yellow) CR (left) and ER (right) pairs in the LFW dataset. Five different resolutions are shown for our baseline model.

resolutions in the ER scenario compared to CR scenario. Further experiments with CFP-FP, AgeDB, CALFW, and CPLFW datasets show the same trend.

## 5 Proposed Network Structures and Training Methods

To improve the separability between features of positive and negative image pairs, and hence, the accuracy, we pursue two intuitive non-transformation-based methods:

- CR batch training (*BT*) with the same network structure as the baseline.
- Siamese network CR training (*ST*) consisting of- and connecting two baseline architectures.

Both approaches are illustrated in Fig. 8. The following two sections will elaborate on them more in detail.

### 5.1 Cross Resolution Batch Training

Motivated by [12, 11], we first propose a straightforward batch CR training approach (*BT*) to tackle the image resolutions. The left part of Fig. 8 illustrates this approach. The architecture is equivalent to our baseline network. Instead of applying only HR images, which we did for the baseline training, we now randomly select half of the HR images per batch and synthetically reduce their resolution (*cf.* Sec. 3.3) of those images. Done that, each batch is containing HR and LR images in the same ratio. In the two-resolution training, we train several specific networks specializing each on a particular resolution. We name these models according to the following rule: *BT* -*r* where *r* denotes the specific LR value during training. To do a more fine-grained analysis at relatively low resolutions we are using the following values for  $r \in [5, 22]$  and according to Sec. 4.3  $r \in \{28, 56\}$ . As we only use half of the images per batch for resolution reduction, all networks still see HR images and learn to extract features for HR and LR images at the same gradient updating step. For all CR batch trainings we use the MS1M dataset and train in total for 16 epochs. All training parameters are set according to our baseline for a fair comparison.

### 5.2 Siamese Network Cross Resolution Training

Inspired by Tang *et al.* [36], we propose a siamese network CR training (*ST*). Therefore, we construct a siamese network structure, as shown in Fig. 8 (right). Generally, each branch of the network is responsible for a specific resolution and all branches share their weights. Thus, the number of parameters is still equal to the baseline. Training with exactly two resolutions HR and LR, requires a two-branch network. Our goal is, that the network projects features from both branches for the same image *I* in different resolutions,  $\mathbf{I}_{\text{HR}}$  and  $\mathbf{I}_{\text{LR}}$  closely together. To enforce this, we add a new loss function to the network, which penalizes the cosine distance between both features. The cosine distance seems reasonable, since we also evaluate the performance later by calculating cosine distance between image pairs. Let  $\mathcal{M}(\cdot)$  be the arcface-network then is  $\mathcal{M}(\mathbf{I}_{\text{HR}})$  a feature from the high-resolution branch. The low-resolution branch generates features  $\mathcal{M}(\mathbf{I}_{\text{LR}})$  for a particular resolution respectively. Our feature distance loss  $\mathcal{L}_{\text{dist}}$  is then:

$$\mathcal{L}_{\text{dist}} = 1 - \sum \left( \frac{\mathcal{M}(\mathbf{I}_{\text{HR}})}{\|\mathcal{M}(\mathbf{I}_{\text{LR}})\|^2} \odot \frac{\mathcal{M}(\mathbf{I}_{\text{HR}})}{\|\mathcal{M}(\mathbf{I}_{\text{LR}})\|^2} \right) \quad (6)$$

For both branches we calculate the cross-entropy classification loss  $\mathcal{L}_{\text{ce}}^{\text{HR}}$  and  $\mathcal{L}_{\text{ce}}^{\text{LR}}$ , respectively. We weigh all three losses approximately equally, we add a factor of 25 to the feature-distance loss. Finally, we conclude the total loss function  $\mathcal{L}$  for the siamese training approach as follows:

$$\mathcal{L} = \mathcal{L}_{\text{ce}}^{\text{HR}} + \mathcal{L}_{\text{ce}}^{\text{LR}} + 25 \cdot \mathcal{L}_{\text{dist}} \quad (7)$$

Due to the siamese network architecture, the training time is about double in the two resolution training scenario. Both images, HR and LR, need to be inferenced through each branch. Therefore, we select the following resolutions  $r \in \{5, 6, 7, 8, 12, 14, 20, 28, 56\}$  to train specific resolution models. For all siamese CR trainings we use MS1M dataset and train for 16 epochs. All training parameters are set according to our baseline to enable a fair comparison.

## 6 Experimental Results

In this section, we present and discuss the results of our proposed approaches. Firstly, we focus on the two-resolution scenario, *i.e.*, HR (112 px) and one specific LR. Secondly, focus on training with multiple image resolutions simultaneously, *i.e.*, HR (112 px) and multiple LRs (7 px, 14 px, 28 px, 56 px and 112 px) in one training. We analyze the accuracy

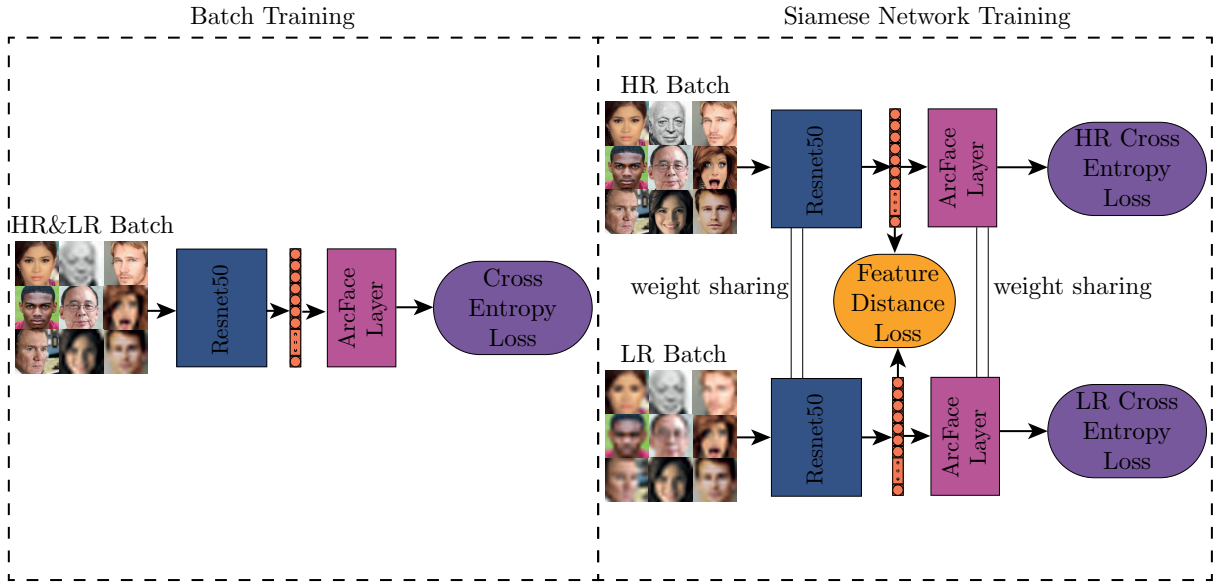


Figure 8: Overview of our proposed methods. The left part shows the CR batch training method (*BT*). The right part shows the siamese network (*ST*) CR training approach.

on five popular datasets and compare the distances of the resulting features for all methods. Moreover, we introduce a new evaluation protocol to measure the performance of a model for multiple resolutions in the test dataset. We are closing this section with a comparison of all in this paper proposed methods, especially concerning the differences in accuracy and training time.

### 6.1 Two Resolution Training Scenario

According to Sec. 5, we now analyze the CR batch training approach *BT* and the siamese network CR training approach *ST* with respect to the face verification accuracy on five popular datasets. In this two-resolution training scenario, we train each model with exactly two specified resolutions and compare the results to the baseline network concerning accuracy and feature distances.

#### Face Verification Accuracy

As introduced in Sec. 3.4, accuracy is a common metric to measure the performance of a face verification model. Fig. 9 depicts the average face verification accuracy across five common datasets of *BT* and *ST* model compared to our baseline model. Note that each data point of *BT* and *ST* represents a different model, which is specifically trained for that resolution. Both approaches clearly outperform the baseline model for low image resolutions. For very low resolutions, *i.e.*, 5 px to 8 px, the performance can be increased from about 50% up to 70%. That is equivalent to a relative improvement of 40%. Above about 40 px image resolution, no significant difference between all approaches is present, which affirms our expectations since the LR images are visually hardly distinguishable from the original images and the absolute pixel difference is very small (*cf.* Sec. 3.3).

Generally, the performance improvement is increasing with decreasing resolutions. The *BT* method performs slightly better than the *ST* method, which leads to the conclusion that the siamese approach might concentrate too much on projecting the features of the same image in different resolution to the same space than on classifying the correct identity regardless of the resolution. For applications with a known fixed resolution, a *BT* is the better choice.

Moreover, we compare our results on the very popular LFW dataset with two other approaches (*cf.* table 1): The selected knowledge distillation technique proposed by Ge *et al.* [32] and the attribute guided coupled GAN approach introduced by Talreja *et al.* [30]. Our systems clearly outperforms both competitors. However, the comparison to Ge *et al.*'s approach is not be fair, their baseline model (teacher model) only reaches an accuracy of 97.15%, which is not comparable to our baseline and state-of-the-art. On the other hand, the model's number of parameters also differs. Both models only trained their models for three different resolutions, which only shows few snapshots and not the whole

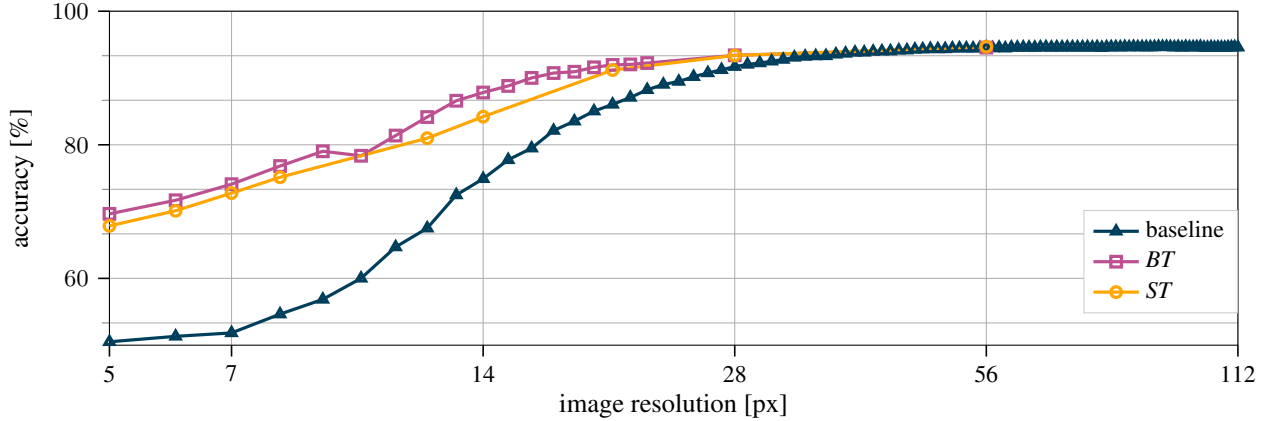


Figure 9: Average face verification accuracy across five popular datasets for different resolution. The baseline (triangles), the *BT* (squares) and *ST* (circles) model are compared.

performance curve. The lowest resolution (16 px) is rather high compared to our analysis, so we cannot fully exploit our strengths here.

### Feature Distances

Similar to Sec. 4, we pick five different resolutions and take a closer look at the features themselves. To be more precise, we plot the distance distributions for positive and negative image pairs from the LFW dataset.

In Fig. 10, on the left side, the distances of extracted features from the *BT* model are plotted and on the right side from *ST* approach, respectively. Distances of positive and negative pairs are much better separable for low resolutions 14 px, 28 px and 56 px than the baseline results (*cf.* Fig. 7). The main difference compared to the baseline is the shift of positive and negative distances to a range of almost 0 and 0.1, in the very low-resolution scenario (7 px). This is remarkable and shows that both networks are actually learning to project features from very different resolutions into the same space. Although the distances are small, still negative distances are larger than positives and the distributions are separable, which is consistent with the accuracy improvement discussed in the previous section (*cf.* Fig. 9). Furthermore, there is no significant difference between both proposed methods, which is also consistent with the previous section’s accuracy values.

To understand and determine the exact resolution at where the feature distances drop so much, we analyze the optimal threshold, which is calculated for the accuracy values (*cf.* Sec. 3.4). Fig. 11 depicts the threshold values for the baseline, *BT*, and *ST* model on all tested image resolution in the CR scenario. Thresholds for our baseline model are increasing for lower resolutions. This is consistent with our results in Sec. 4.3, where both positive and negative feature distances

Table 1: Face verification accuracy on the LFW dataset. Best performance of each image resolution is marked bold.

image resolution	model	accuracy
64 px	<i>BT</i> -64 (ours)	<b>99.38%</b>
	<i>ST</i> -64 (ours)	99.35%
	S-64-sc [32]	92.83%
	Talreja <i>et al.</i> [30]	94.92%
32 px	<i>BT</i> -32 (ours)	<b>99.08%</b>
	<i>ST</i> -32 (ours)	98.32%
	S-32-sc [32]	89.72%
	Talreja <i>et al.</i> [30]	91.08%
16 px	<i>BT</i> -16 (ours)	<b>98.17%</b>
	<i>ST</i> -16 (ours)	97.8%8
	S-16-sc [32]	85.87%

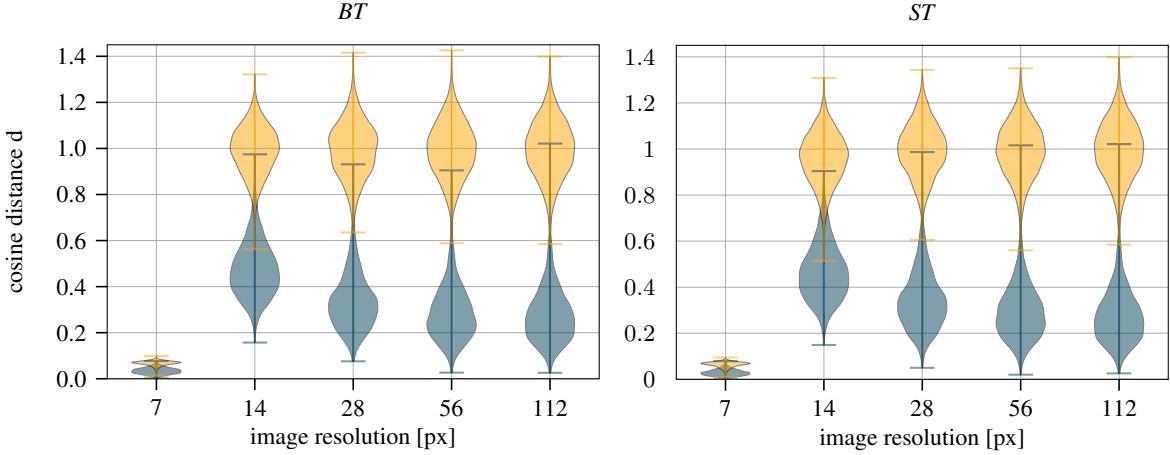


Figure 10: Cosine feature distance distributions for positive (blue) and negative (yellow) CR pairs in the LFW dataset. Five different resolutions are compared for *BT* (left) and *ST* (right).

increase for lower resolutions. Both of our two-resolution training networks show a significant drop, at a resolution of 9 px for *BT* and approximately 12 px for *ST*. From these points on, both models are training differently and projecting features for large resolution differences more closely together. There is no connection between this drop in feature distances and the performance of both models conductible.

## 6.2 Multi-Resolution Training Scenario

To simulate a more applicable model, which is capable of handling arbitrary resolutions, we propose a multiple-resolution training for both of our previously presented approaches. We train the *BT* model with more than two resolutions at the same time by simply randomly pick a different resolution from the numbers  $\{7, 14, 28, 56, 112\}$  for generating a LR image. Each batch contains multiple LR images with different resolutions and HR images. We find that those five resolutions equally represent the range of image resolutions. This reflects, for example, equivalent distances from subjects to camera in real life. The probability of each resolution is set to be equal. We name this approach *BT-M* in the following.

In the *ST* approach, we apply two different methods for training with multiple resolutions simultaneously. First, for the LR branch, we simply randomly pick a resolution from the numbers  $\{7, 14, 28, 56\}$  and feed the LR branch with different resolution LR images within each batch. The HR branch always takes 112 px images. Hence, we only double the training time but train with in total five different resolutions simultaneously. That approach will be referred to as *ST-M2* in the following. The second method *ST-M2* extends the siamese network to in total to five branches, each branch representing a certain defined resolution (7 px, 14 px, 28 px, 56 px, and 112 px). Consequently, five feature distance losses are calculated each between the HR and the corresponding LR branch. Moreover, we also calculate the

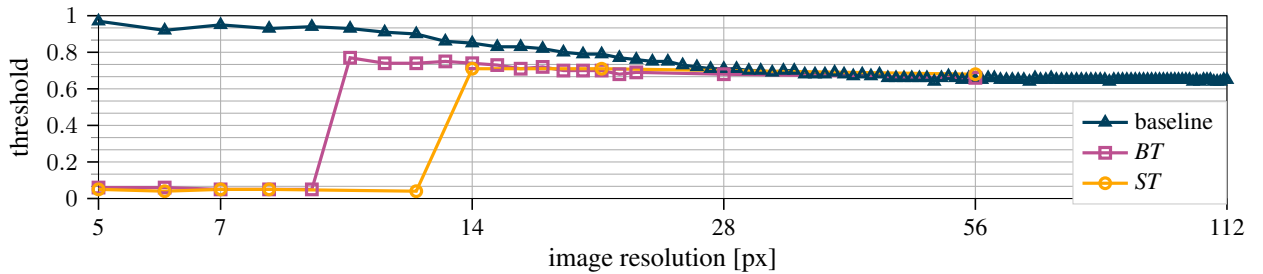


Figure 11: Best threshold values for calculating the CR accuracy on the LFW datasets using baseline (diamonds), *BT* (squares) and *ST* (circles) models.

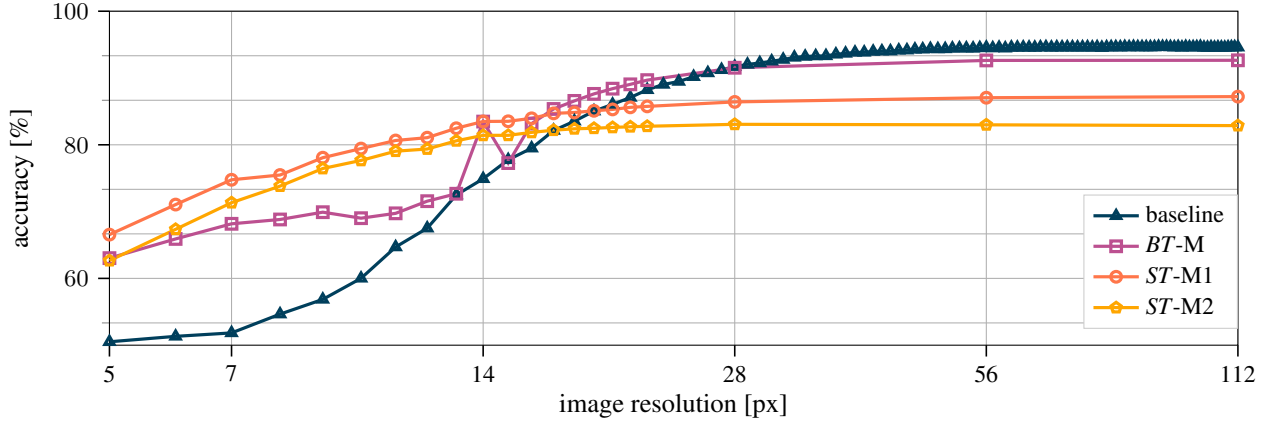


Figure 12: Average face verification accuracy across five popular datasets for different image resolutions. The baseline (diamonds), the *BT-M* (squares), *ST-M1* (circles), and *ST-M2* (pentagons) model are compared.

cross-entropy loss for each branch. All feature distance losses are weighted with a factor of 3 to be in the same order of magnitude as the cross-entropy losses. The training time for this experiment is about five times longer than the baseline because it is scaling with the number of defined resolutions for training.

### Face Verification Accuracy

In Fig. 12, we present the face verification accuracy for *BT-M*, *ST-M1*, and *ST-M2* model across arbitrary image resolutions. All three approaches perform significantly better than the baseline model in resolutions below 13 px and worse above a resolution of 28 px. Note that there is a significant peak at a resolution of 14 px, especially for *BT-M*. One reason for this could be, that this specific resolution was in the training resolution included. This effect is not visible at a resolution of 7 px, 28 px, and 56 px. Another finding we can conduct is that the siamese network CR training outperforms the CR batch training for low resolutions (approx. below 16 px) and vice-versa for mid and high resolutions (approx. above 16 px). At a low resolution of 7 px the *ST-M1* model achieves an accuracy score of about 75%, that is almost 25% above the baseline performance. At the same time, that approach loses about 8% performance at high resolutions like 56 px. For a more scale comprehensive performance score, we will introduce three new evaluation protocols in Sec. 6.3.

In Fig. 13 we investigate the performance at and close to two selected resolutions 7 px and 14 px. On the left side we can see that *BT-7* and *ST-7* optimized the performance exactly for the 7 px resolution, hence they perform worse in the neighboring regions. Obviously, *BT-5-9* and *ST-5-8*, which both represent specific resolution trained models, performing best at each scale. This is reasonable due to the training with that particular image resolution. The performance loss for all multiple-resolution trained approaches (*BT-M*, *ST-M1*, and *ST-M2*) is compensated by the benefit of having a single model for arbitrary resolutions. The right part of Fig. 13 shows an excerpt of resolutions from 10 px and 18 px. In other words, it illustrates the neighboring region of a 14 px image resolution. Here, the wave effect of *BT-14* and *ST-14* is also present, meaning that those two models perform relatively best on exactly 14 px resolution. Remarkable is a significant peak in accuracy for *BT-M* model at the focused resolution of 14 px. The for each specific trained two-resolution networks *BT-10-18* is performing best on all scales.

### Feature Distances

Interestingly, in terms of feature distance distributions (*cf.* left part of Fig. 14), the multi-resolution batch training is not behaving similarly to the two resolution batch training. Specifically for *BT*, at very low resolutions (7 px), the feature distance distributions for positive and negative pairs are even larger than for all other resolutions. This fits together with the *BT* accuracy at that scale (*cf.* Fig. 13). In contrast to the two-resolution case, both siamese training approaches (*ST-M1* and *ST-M2*) project features for all resolutions more closely together. We conduct this from very low distances across all scales (middle and right part in Fig. 14). The maximum feature distance for both approaches is about 0.1.

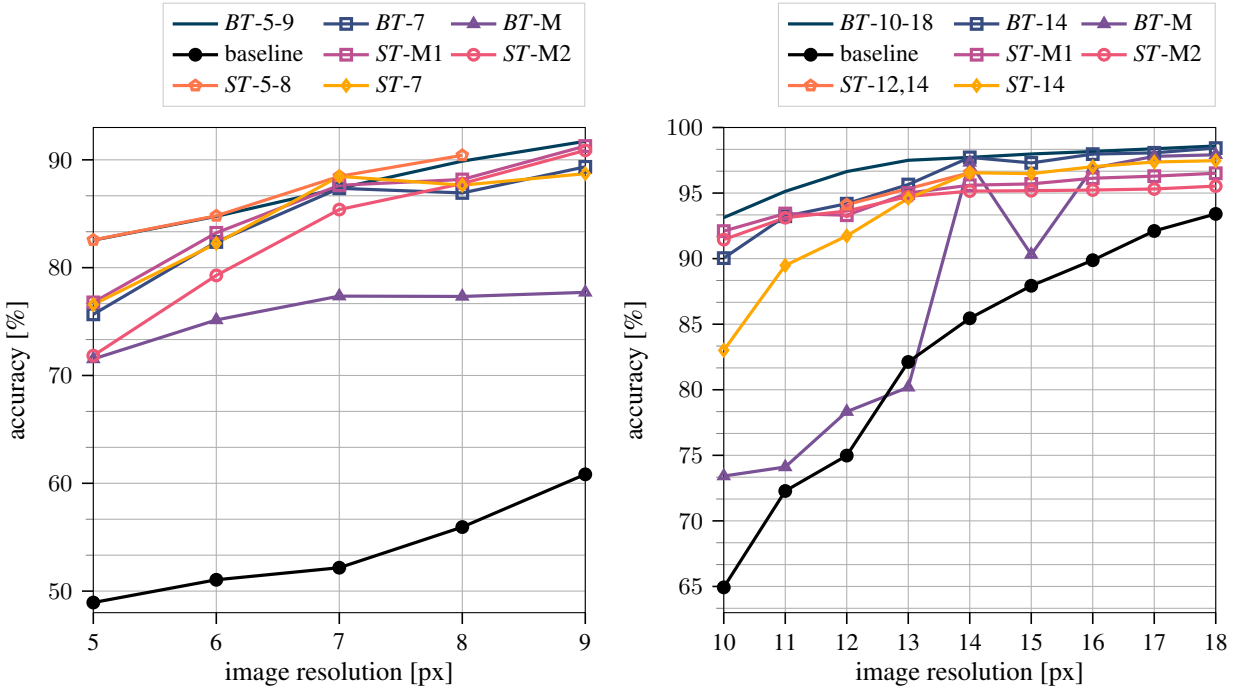


Figure 13: Accuracy for LFW dataset in the region of 5 px and 9 px (left) and 10 px and 18 px (right.)

### 6.3 Evaluation Protocols for Multiple Resolutions

Evaluation protocols for common public datasets are not taking the image resolution into account. In the previous sections, we only considered a specific image resolution to calculate the face verification accuracy. With single networks (*cf.* Sec. 6.2) capable of handling arbitrary image resolutions at once, there is a need for a more meaningful evaluation considering multiple resolutions. Therefore, we propose evaluation protocols for all five datasets. We focus on three different resolution ranges:

- Low resolution: Resolutions in the range of 5 px to 10 px are randomly picked with each with the same probability for the LR images in the CR evaluation. That means we derive a list containing the resolution for each image in each pair for the corresponding dataset.
- Mid resolution: Resolutions in the range of 10 px to 40 px are used for selection.
- High resolution: Resolutions in the range of 40 px to 112 px are used for selection.

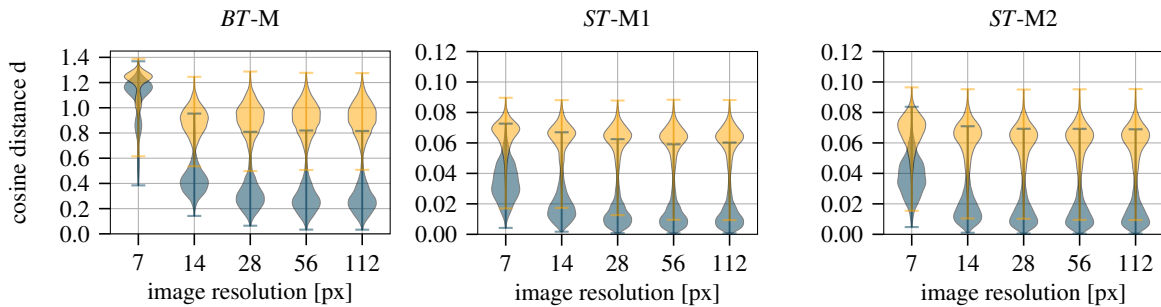


Figure 14: Cosine feature distance distributions for positive (blue) and negative (yellow) CR pairs in the LFW dataset. Five different resolutions are compared for BT-M (left), ST-M1 (center), and ST-M2 (right).

Moreover, we generate a protocol that takes every single resolution in the range of 5 px to 112 px into account. This will be referred to as *all\_res* in table 2. All evaluation protocols are published and available on GitHub<sup>2</sup>.

#### 6.4 Comparison of the proposed Methods

Finishing this chapter, a comparison between all introduced methods is given. First, we analyze the verification performance on HR images for both proposed methods and compare them to the baseline approach. Fig. 15 shows the accuracy of the LFW dataset for each epoch. We select the models *BT-7*, *BT-56* and *ST-7*, *ST-56* to represent a very low and relatively high resolution. After the first epoch our baseline model achieves about 98% accuracy, followed by almost peak accuracy already after the second epoch. During epochs 3 and 16, no significant changes in accuracy are visible. The *BT-56* starts with equal accuracy after the first epoch and then takes another two epochs to reach almost peak accuracy. The *ST-56* gets only after epoch 4 approximately peak performance. This model needs significantly more samples than both previously mentioned models to achieve similar accuracy. One reason for that could be the additional feature distance loss, which forces the network to additionally concentrate on minimizing feature distances and not only learn a good classification.

The peak performance for both methods *BT-7* and *ST-7* is significantly lower compared to the other approaches. This could evolve from too little information in the very low LR images, which might probably be just too less resolution to be able to learn a proper feature extraction. Moreover, the speed of learning is clearly slower. To get close to the maximum accuracy, both approaches need at least 10 epochs.

Second, table 2 compares all presented methods towards their training time per epoch and performance in the two-resolution scenario and multi-resolution scenario and depicts accuracy values on the LFW dataset. We conduct that compared to the two resolution techniques, both *ST-M1* and *ST-M2* models clearly outperform the baseline and the *BT-M* for low resolutions. Focusing on higher resolutions, the *BT-M* method is performing best. Even for the original image resolution of 112 px, the *BT-M* model performs better than the baseline. We think this is reasonable because using lower resolutions additionally during training can be seen as an extra data augmentation and hence, can improve the performance. One also has to compromise that for a performance improvement of about absolute 14% in the *low\_res* protocol, the performance for *high\_res* drops about 2%. The second siamese training approach, *ST-M2* is performing worse in all categories than *ST-M1*. Therefore, we conclude that the much greater effort for training is not worth it. It seems to be less essential to force a network to learn close features for the same image in different resolutions, within each batch, than across several batches.

Lastly, the inference time and the number of parameters are equal for all models, which make the comparison fair and reasonable.

<sup>2</sup><https://github.com/Martlgap/btm-stm>

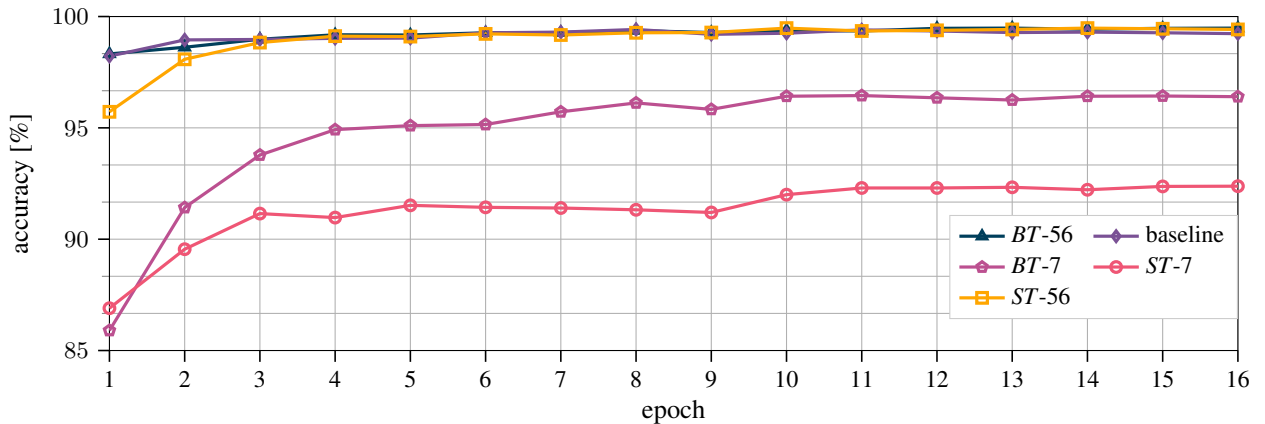


Figure 15: Accuracy scores for 112 px resolution testing on the LFW dataset of the baseline (diamonds), *BT-56* (triangles), *BT-7* (pentagons) and *ST-56* (squares), and *ST-7* (circles) after each training epoch.



Table 2: Comparison in terms of training time per epoch and accuracy on LFW dataset for different resolution protocols. Bold numbers denote the best performance across all methods.

		baseline	<i>BT</i> -5	<i>BT</i> -M	<i>ST</i> -5	<i>ST</i> -M1	<i>ST</i> -M2
training time		2 h	2 h	2 h	4 h	4 h	20 h
	112 px	99.23%		<b>99.30%</b>		97.40%	95.62%
	all_res	96.86%		<b>97.72%</b>		96.76%	95.07%
accuracy	high_res	99.20%	.	<b>99.33%</b>	.	97.35%	95.62%
	mid_res	95.89%		<b>97.78%</b>		96.98%	95.51%
	low_res	77.57%		87.17%		<b>91.50%</b>	88.72%
	5 px	54.65%	69.66%	71.53%	67.86%	<b>76.78%</b>	71.84%

## 7 Conclusions and Future Work

In this work, we analyze the impact of different image resolutions on face verification performance using a state-of-the-art approach. The distances between extracted features are deeply analyzed. Our findings are that features of classical face recognition networks are not scale-invariant. The performance decreases heavily for lower resolutions.

To achieve best performance, the image resolution requires to be the same as in the corresponding training dataset for the network. To overcome this problem, we propose two intuitive methods to learn scale-invariant features directly. 1) *BT* describes training our network with batches containing LR and HR images in the same ratio. 2) *ST* is a siamese network structure constructed from a state-of-the-art network. This approach is moreover using feature-distances between LR and HR version of the same image as an additional loss to minimize these distances besides optimizing the classification problem. We demonstrate that our models can clearly improve CR face verification accuracy on five standard datasets.

Moreover, we train our proposed models with several resolutions at once. Hence, a single model can be applied to arbitrary image scales. We also report considerable improvements for CR verification performance, especially for low resolutions.

Lastly, we introduce three different evaluation protocols for five popular datasets, considering multiple resolutions in the face verification evaluation process for CR scenarios.

In the future, we plan to focus more on minimizing the intra-class feature-distance between LR and HR images to improve the robustness of features furthermore. Moreover, the inter-class distances between LR and HR images should be further maximized. Therefore, we consider adding and adapting a triplet loss function to our networks. We also want to extend the downsample process by using arbitrary blur kernels like described in [37] and apply it in our work.

## References

- [1] Yandong Guo, Lei Zhang, Yuxiao Hu, Xiaodong He, and Jianfeng Gao, “Ms-celeb-1m: A dataset and benchmark for large-scale face recognition,” in *European conference on computer vision*. Springer, 2016, pp. 87–102.
- [2] Christian Szegedy, Wei Liu, Yangqing Jia, Pierre Sermanet, Scott Reed, Dragomir Anguelov, Dumitru Erhan, Vincent Vanhoucke, and Andrew Rabinovich, “Going deeper with convolutions,” in *Proceedings of the IEEE conference on computer vision and pattern recognition*, 2015, pp. 1–9.
- [3] Pei Li, Loreto Prieto, Domingo Mery, and Patrick J Flynn, “On low-resolution face recognition in the wild: Comparisons and new techniques,” *IEEE Transactions on Information Forensics and Security*, vol. 14, no. 8, pp. 2000–2012, 2019.
- [4] Zhiyi Cheng, Xiatian Zhu, and Shaogang Gong, “Low-resolution face recognition,” *CoRR*, vol. abs/1811.08965, 2018.
- [5] Omid Abdollahi Aghdam, Behzad Bozorgtabar, Hazim Kemal Ekenel, and Jean-Philippe Thiran, “Exploring factors for improving low resolution face recognition,” in *2019 IEEE/CVF Conference on Computer Vision and Pattern Recognition Workshops (CVPRW)*. IEEE, 2019, pp. 2363–2370.
- [6] Maneet Singh, Shruti Nagpal, Richa Singh, Mayank Vatsa, and Angshul Majumdar, “Magnifyme: Aiding cross resolution face recognition via identity aware synthesis,” *arXiv preprint arXiv:1802.08057*, 2018.
- [7] Kaipeng Zhang, Zhanpeng Zhang, Chia-Wen Cheng, Winston H Hsu, Yu Qiao, Wei Liu, and Tong Zhang, “Super-identity convolutional neural network for face hallucination,” in *Proceedings of the European conference on computer vision (ECCV)*, 2018, pp. 183–198.

- [8] Berk Dogan, Shuhang Gu, and Radu Timofte, “Exemplar guided face image super-resolution without facial landmarks,” in *Proceedings of the IEEE Conference on Computer Vision and Pattern Recognition Workshops*, 2019, pp. 0–0.
- [9] Nasrabadi NM et al., “Identity-aware deep face hallucination via adversarial face verification,” in *IEEE International Conference on Biometrics Theory Applications and Systems*, 2019.
- [10] Chih-Chung Hsu, Chia-Wen Lin, Weng-Tai Su, and Gene Cheung, “Sigan: Siamese generative adversarial network for identity-preserving face hallucination,” *IEEE Transactions on Image Processing*, vol. 28, no. 12, pp. 6225–6236, 2019.
- [11] Fabio Valerio Massoli, Giuseppe Amato, and Fabrizio Falchi, “Cross-resolution learning for face recognition,” *Image and Vision Computing*, p. 103927, 2020.
- [12] Dan Zeng, Hu Chen, and Qijun Zhao, “Towards resolution invariant face recognition in uncontrolled scenarios,” in *2016 International Conference on Biometrics (ICB)*. IEEE, 2016, pp. 1–8.
- [13] E. G. Huang, G. B. Learned-Miller, “Labeled Faces in the Wild: Updates and New Reporting Procedures,” Tech. Rep. UM-CS-2014-003, University of Massachusetts, Amherst, May 2014.
- [14] Stylianos Moschoglou, Athanasios Papaioannou, Christos Sagonas, Jiankang Deng, Irene Kotsia, and Stefanos Zafeiriou, “Agedb: the first manually collected, in-the-wild age database,” in *Proceedings of the IEEE Conference on Computer Vision and Pattern Recognition Workshops*, 2017, pp. 51–59.
- [15] Soumyadip Sengupta, Jun-Cheng Chen, Carlos Castillo, Vishal M Patel, Rama Chellappa, and David W Jacobs, “Frontal to profile face verification in the wild,” in *2016 IEEE Winter Conference on Applications of Computer Vision (WACV)*. IEEE, 2016, pp. 1–9.
- [16] Tianyue Zheng, Weihong Deng, and Jiani Hu, “Cross-age lfw: A database for studying cross-age face recognition in unconstrained environments,” *arXiv preprint arXiv:1708.08197*, 2017.
- [17] Tianyue Zheng and Weihong Deng, “Cross-pose lfw: A database for studying cross-pose face recognition in unconstrained environments,” *Beijing University of Posts and Telecommunications, Tech. Rep.*, vol. 5, 2018.
- [18] Jiankang Deng, Jia Guo, Niannan Xue, and Stefanos Zafeiriou, “Arcface: Additive angular margin loss for deep face recognition,” in *Proceedings of the IEEE Conference on Computer Vision and Pattern Recognition*, 2019, pp. 4690–4699.
- [19] Florian Schroff, Dmitry Kalenichenko, and James Philbin, “Facenet: A unified embedding for face recognition and clustering,” in *Proceedings of the IEEE conference on computer vision and pattern recognition*, 2015, pp. 815–823.
- [20] Weiyang Liu, Yandong Wen, Zhiding Yu, Ming Li, Bhiksha Raj, and Le Song, “Sphereface: Deep hypersphere embedding for face recognition,” in *Proceedings of the IEEE conference on computer vision and pattern recognition*, 2017, pp. 212–220.
- [21] Hao Wang, Yitong Wang, Zheng Zhou, Xing Ji, Dihong Gong, Jingchao Zhou, Zhifeng Li, and Wei Liu, “Cosface: Large margin cosine loss for deep face recognition,” in *Proceedings of the IEEE Conference on Computer Vision and Pattern Recognition*, 2018, pp. 5265–5274.
- [22] Yonghyun Kim, Wonpyo Park, Myung-Cheol Roh, and Jongju Shin, “Groupface: Learning latent groups and constructing group-based representations for face recognition,” in *Proceedings of the IEEE/CVF Conference on Computer Vision and Pattern Recognition*, 2020, pp. 5621–5630.
- [23] Qiangchang Wang, Tianyi Wu, He Zheng, and Guodong Guo, “Hierarchical pyramid diverse attention networks for face recognition,” in *Proceedings of the IEEE/CVF Conference on Computer Vision and Pattern Recognition*, 2020, pp. 8326–8335.
- [24] Ruofan Zhou and Sabine Susstrunk, “Kernel modeling super-resolution on real low-resolution images,” in *Proceedings of the IEEE International Conference on Computer Vision*, 2019, pp. 2433–2443.
- [25] Robert Keys, “Cubic convolution interpolation for digital image processing,” *IEEE transactions on acoustics, speech, and signal processing*, vol. 29, no. 6, pp. 1153–1160, 1981.
- [26] Zhifei Wang, Zhenjiang Miao, QM Jonathan Wu, Yanli Wan, and Zhen Tang, “Low-resolution face recognition: a review,” *The Visual Computer*, vol. 30, no. 4, pp. 359–386, 2014.
- [27] Ze Lu, Xudong Jiang, and Alex Kot, “Deep coupled resnet for low-resolution face recognition,” *IEEE Signal Processing Letters*, vol. 25, no. 4, pp. 526–530, 2018.
- [28] Erfan Zangeneh, Mohammad Rahmati, and Yalda Mohsenzadeh, “Low resolution face recognition using a two-branch deep convolutional neural network architecture,” *Expert Systems with Applications*, vol. 139, pp. 112854, 2020.

- [29] Vahid Reza Khazaie, Nicky Bayat, and Yalda Mohsenzadeh, “Ipu-net: Multi scale identity-preserved u-net for low resolution face recognition,” *arXiv preprint arXiv:2010.12249*, 2020.
- [30] Veeru Talreja, Fariborz Taherkhani, Matthew C Valenti, and Nasser M Nasrabadi, “Attribute-guided coupled gan for cross-resolution face recognition,” *arXiv preprint arXiv:1908.01790*, 2019.
- [31] Sivaram Prasad Mudunuri, Soubhik Sanyal, and Soma Biswas, “Genlr-net: Deep framework for very low resolution face and object recognition with generalization to unseen categories,” in *2018 IEEE/CVF Conference on Computer Vision and Pattern Recognition Workshops (CVPRW)*. IEEE, 2018, pp. 602–60209.
- [32] Shiming Ge, Shengwei Zhao, Chenyu Li, and Jia Li, “Low-resolution face recognition in the wild via selective knowledge distillation,” *IEEE Transactions on Image Processing*, vol. 28, no. 4, pp. 2051–2062, 2018.
- [33] Kaiming He, Xiangyu Zhang, Shaoqing Ren, and Jian Sun, “Deep residual learning for image recognition,” in *Proceedings of the IEEE conference on computer vision and pattern recognition*, 2016, pp. 770–778.
- [34] Olga Russakovsky, Jia Deng, Hao Su, Jonathan Krause, Sanjeev Satheesh, Sean Ma, Zhiheng Huang, Andrej Karpathy, Aditya Khosla, Michael Bernstein, et al., “Imagenet large scale visual recognition challenge,” *International journal of computer vision*, vol. 115, no. 3, pp. 211–252, 2015.
- [35] Yandong Wen, Kaipeng Zhang, Zhifeng Li, and Yu Qiao, “A discriminative feature learning approach for deep face recognition,” in *European conference on computer vision*. Springer, 2016, pp. 499–515.
- [36] Su Tang, Shan Zhou, Wenxiong Kang, Qiuxia Wu, and Feiqi Deng, “Finger vein verification using a siamese cnn,” *IET Biometrics*, vol. 8, no. 5, pp. 306–315, 2019.
- [37] Kai Zhang, Wangmeng Zuo, and Lei Zhang, “Deep plug-and-play super-resolution for arbitrary blur kernels,” in *Proceedings of the IEEE Conference on Computer Vision and Pattern Recognition*, 2019, pp. 1671–1681.